

Review

Laser Absorption Sensing Systems: Challenges, Modeling, and Design Optimization

Zhenhai Wang ¹, Pengfei Fu ² and Xing Chao ^{1,*}

¹ Center for Combustion Energy, Department of Energy and Power Engineering and Key Laboratory for Thermal Science and Power Engineering of Ministry of Education, Tsinghua University, Beijing 100084, China

² School of Aerospace Engineering, Tsinghua University, Beijing 100084, China

* Correspondence: chaox6@tsinghua.edu.cn; Tel.: +86-10-6278-4497

Received: 31 May 2019; Accepted: 3 July 2019; Published: 5 July 2019



Abstract: Laser absorption spectroscopy (LAS) is a promising diagnostic method capable of providing high-bandwidth, species-specific sensing, and highly quantitative measurements. This review aims at providing general guidelines from the perspective of LAS sensor system design for realizing quantitative species diagnostics in combustion-related environments. A brief overview of representative detection limits and bandwidths achieved in different measurement scenarios is first provided to understand measurement needs and identify design targets. Different measurement schemes including direct absorption spectroscopy (DAS), wavelength modulation spectroscopy (WMS), and their variations are discussed and compared in terms of advantages and limitations. Based on the analysis of the major sources of noise including electronic, optical, and environmental noises, strategies of noise reduction and design optimization are categorized and compared. This addresses various means of laser control parameter optimization and data processing algorithms such as baseline extraction, *in situ* laser characterization, and wavelet analysis. There is still a large gap between the current sensor capabilities and the demands of combustion and engine diagnostic research. This calls for a profound understanding of the underlying fundamentals of a LAS sensing system in terms of optics, spectroscopy, and signal processing.

Keywords: laser absorption spectroscopy (LAS); combustion sensing; direct absorption spectroscopy (DAS); wavelength modulation spectroscopy (WMS); design optimization; noise reduction algorithms

1. Introduction

1.1. Overview of Laser Absorption Sensor Developments and Applications

Laser absorption spectroscopy (LAS) has served as a useful tool for both fundamental and practical studies in energy and power systems since its earliest demonstration as a species diagnostic method in combustion-related environments over forty years ago [1,2]. In addition to the non-contact characteristics of most optically based methods (e.g., emission, Schlieren imaging, laser-induced fluorescence, particle image velocimetry), LAS benefits from the species-specific nature of molecular spectroscopy, therefore is capable of achieving highly quantitative and selective measurements of a number of important species parameters including gas composition, temperature, pressure, and velocity. The use of narrow-linewidth, tunable, low-power semiconductor lasers, on the other hand, offers the opportunity for real-time, time-resolved, and long-term stable field monitoring systems that can be realized under various measurement scenarios.

Up towards the early 2000s, gas sensors based on tunable diode laser absorption spectroscopy (TDLAS) were extensively applied in continuous emission monitoring and process controls and diffused in process industries as an accepted technique [3,4]. The maturity and commercialization

of opto-electronic devices, thanks to the booming telecommunication industry, has allowed TDLAS sensors to evolve from laboratory-scale benchtop experimental tools to a robust industrial technology. With further reduction in cost and size, portable and field-deployable systems can be made. Using smart optical–mechanical designs and sophisticated signal processing schemes, some of these sensors are able to operate in the field without operator intervention for over 10 years [5].

Today, the design, control, and optimization of complex energy and propulsion systems poses unprecedented challenges for sensor technology. The extreme conditions associated with combustion that are typically unfriendly for optical systems, such as high temperature, pressure, and velocity, mechanical vibrations, high dust levels, and corrosiveness, make LAS still one of the best available contactless sensor techniques for harsh environments. However, extraction and interpretation of high-quality, quantitative information under such complicated, demanding conditions requires deeper understanding of the target environments and tailoring the sensor design to specific measurement goals. While state-of-the-art laser technology for novel single-mode mid-infrared and hyperspectral laser sources continues to offer much more freedom in choosing the spectral features and designing LAS sensors, much remains to be studied in improving their reliability, accuracy, and precision.

1.2. Scope and Organization of the Paper

There has been a number of excellent reviews and books on the development and application of LAS sensor technology. Even as early as in the late 1990s, several papers reviewed the fundamental theories and early successes of laser-based spectroscopic methods in gas dynamics and combustion flow measurements [6–8]. Nasim et al. illustrated the evolution of and confinement methods used in semiconductor diode lasers and discussed different techniques used to convert free-running diode lasers into true narrow linewidth tunable diode laser sources [9]. As lasers were much less mature at that time, these papers also reviewed the available laser light sources as an important part of the diagnostics development. More recently, several reviews reported the advances of the LAS technique and its demonstration in various disciplines. Hanson et al. presented an overview of combustion kinetics, propulsion, and combustion in practical systems and documented the impact of quantitative laser diagnostics methods [10]. Bolshov et al. highlighted the temperature, concentrations, and flow velocities in different combustion zones and emphasized the strategies and data processing algorithms for LAS measurements [11]. Goldenstein et al. provided a thorough review of the underlying fundamentals, design, and use of infrared LAS sensors for combustion gases and highlighted recent findings and some of the remaining measurement opportunities, challenges, and needs [12]. Liu et al. summarized the key principles and recent advances of line-of-sight (LOS) LAS techniques and then focused on spatially resolved gas sensing with LAS tomography [13].

More specifically, a few papers have focused on reviewing signal-to-noise-ratio (SNR) enhancement techniques to improve TDLAS performance. Li et al. summarized several commonly employed noise reduction schemes including signal averaging, modulation techniques, balanced detection, zero-background subtraction, and adaptive filtering [14]. Zhang et al. focused on the various mathematical algorithms applied in TDLAS signal processing to enhance the accuracy and resolution of the sensor [15].

As discussed above, sensing challenges vary largely with measurement targets and conditions. The maturity of semiconductor lasers and photodetectors allows many researchers in relevant fields to simply use LAS sensor as an established tool, whereas diagnosticians still strive to push the limit of this technique. While previous papers have provided comprehensive reviews on all major elements of LAS sensor systems including fundamental molecular spectroscopy, the development of opto-electronic devices, and various measurement schemes and applications, we refer the readers to other works for the fundamentals and will address the design perspectives of a LAS sensing system. Section 2 will start by summarizing and identifying the measurement challenges and design targets under different measurement conditions; Section 3 will follow by outlining the fundamentals of different diagnostic strategies and their underlying models and control factors; Section 4 will then provide a systematic

analysis of approaches for noise reduction and signal optimization, so to extend the use of the LAS sensing technique to much more difficult measurement scenarios. In view of the urging demands in both the use and development of this sensor technology, a goal of this manuscript is to provide understanding and an overview of the key factors and considerations in the measurement targets, as well as a reference and guidelines to a strategic design procedure appropriate for obtaining optimized sensing results.

2. Sensor Design Targets and Measurement Challenges

The fundamental theory lying behind absorption spectroscopy is the Beer–Lambert law, presented in Equation (1), with multiple forms of expressions. The fractional transmission of light, given by the ratio between transmitted and incident light intensity, I_t [W/cm^2] and I_0 [W/cm^2], can be expressed as an exponential function of absorbance α_ν , with k_ν [$1/\text{cm}$] being the spectral absorption coefficient, L [cm] the absorption pathlength, n [$\text{molecule}/\text{cm}^3$] the number density of the absorbing species, σ_ν [$\text{cm}^2/\text{molecule}$] the absorption cross section, S [$\text{cm}^{-2}/\text{atm}$] the absorption linestrength of an individual transition line, ϕ_ν [cm] the frequency-dependent lineshape function, P [atm] the total pressure, and X_i the mole fraction of the absorbing species i . The subscript ν is used to signify the spectral dependence of the parameter on the light frequency ν :

$$\begin{aligned} (I_t/I_0)_\nu &= \exp(-\alpha_\nu) \\ &= \exp(-k_\nu L) \\ &= \exp(-n\sigma_\nu L) \\ &= \exp(-S\phi_\nu P X_i L) \end{aligned} \quad (1)$$

This rather simple but nontrivial relationship roots from the energy balance derivation in the equation of radiative transfer. In a typical absorption measurement, the total absorbance α_ν is the ultimate “signal” to optimize, and the performance of LAS species sensor is commonly evaluated through detection limits and detection bandwidth. The limits of detection can be quantified as the noise-equivalent absorbance (NEA) or the minimal detectable concentration (e.g., in ppm), and the measurement bandwidth (Hz) can be defined as half of the measurement temporal resolution taking into account the Nyquist criterion.

To directly compare the detectivity of LAS sensors under different measurement conditions, the pathlength-normalized detection limit (e.g., in ppm·m) is often used, on the basis of the fact that the absorbance is linearly proportional to the absorption pathlength. Further normalization with bandwidth renders a detection limit in the unit of $\text{ppm}\cdot\text{m}\cdot\text{Hz}^{-1/2}$ to account for the improvement of signal-to-noise ratio (SNR) with averaging. However, it needs to be noted that this inverse square-root dependence on averaging time can be applied if the signal carries only white noise. A more rigorous assessment of the validity of such normalization can be done with Allan variance analysis, which analyzes a sequence of data in the time domain. Although traditionally used as a measure of frequency stability of clocks and oscillators in metrology, the Allan variance analysis can also be adopted as a useful tool to identify and quantify different noise terms and indicate signal stability. As shown in the schematic of Figure 1, the root Allan variance, aka Allan deviation, of a time domain signal is computed as a function of different averaging times τ . By analyzing the characteristic regions and log–log scale slopes of the Allan deviation curve, different noise processes and modes may be identified.

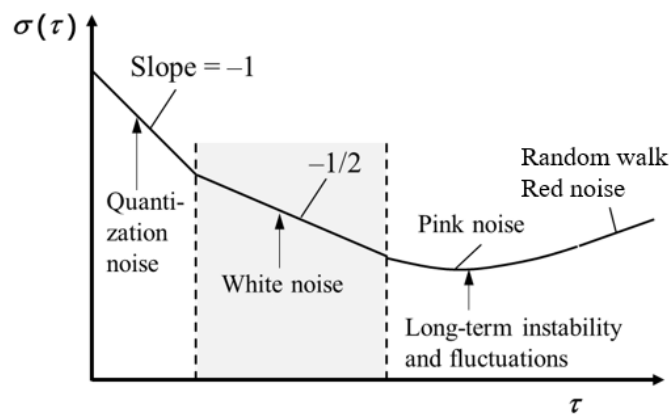


Figure 1. Schematic of different noise processes on an Allan deviation plot.

Even limiting our discussion to combustion-related LAS diagnostic studies, the demands and achieved performance of the laser sensors vary over a wide range. Figure 2 summarizes some representative results from a number of sensor development and implementation studies in terms of detection limits and bandwidths. It compares species concentration measurements in a variety of combustion systems including laboratory environments [1,16–22], shock tube studies [23–28], industry processes [29–33], and engines [34–46]. For the purpose of making a direct comparison between different studies, the reported absolute minimal detection limits for several commonly probed species in combustion, including CO, CO₂, H₂O, and C₂H₂, are plotted on the same diagram against detection bandwidths. It can be clearly observed that results from different applications naturally separate into different regimes: the well-controlled laboratory environments allow lower absorbance to be detected, where chemical kinetics studies in shock tubes typically demand for a much higher detection bandwidth than stabilized laboratory flames or gas cell; larger scale, more “realistic” environments such as industrial burners and engines present harsher conditions that lead to higher achievable minimal detection limits, but industrial process monitoring typically involves stringent emission control targets and trace species detection over continuous, long-term monitoring periods, whereas engine diagnostics are usually associated with high-velocity or turbulent flow and reaction conditions.

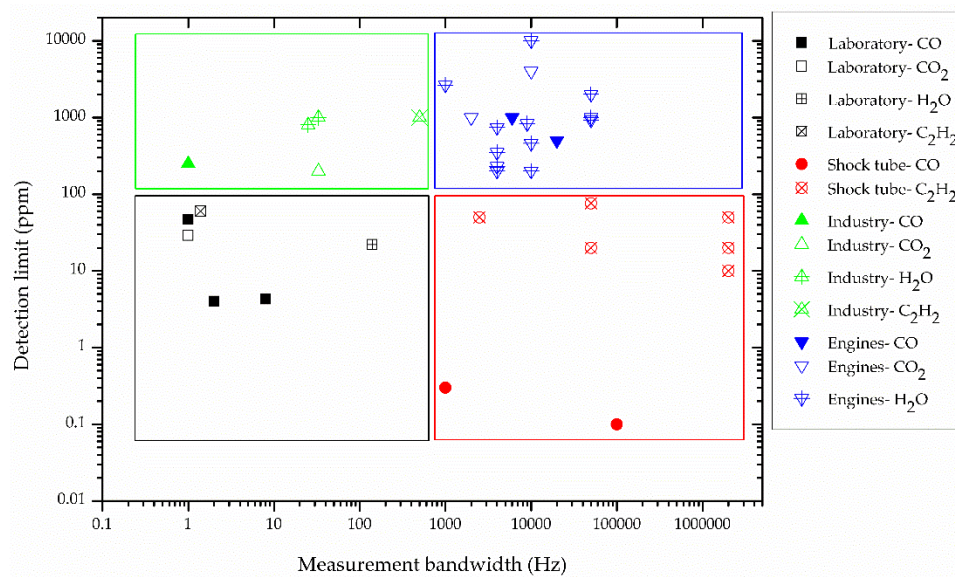


Figure 2. Representative detection limits and measurement bandwidths of laser absorption sensors in various combustion-related systems.

Despite its versatility in measuring temperature, pressure, and velocity, LAS is ultimately a species diagnostic method. It utilizes the “fingerprint” molecular spectra and infer the parameters to be measured on the basis of a correct interpretation of the recorded spectral feature. Figure 3 plots the absorption linestrengths over the infrared wavelength range of 0.5–6 μm of several of the representative C–O, C–H, N–O, N–H, and H–O compound gaseous species commonly studied in combustion. Today, with semiconductor laser technology, we are able to access almost any wavelength within this region, so that there is no longer much constraint in making an optimized selection of absorption transition, which can be solely based on appropriate strength level and minimal cross interference. For fairly harmonic molecules such as CO, the advantage of using a lower-order vibrational band at longer wavelength is more prominent in achieving lower detection limits as compared with a less harmonic molecule such as NH_3 . One can also make the observation that high temperatures, often associated with combustion-related sensing, would by themselves present greater challenges for LAS sensors. The reasoning is twofold from the point of view of molecular spectroscopy: (1) the overall band strength is approximately inversely proportional to temperature, so that absorption is generally weaker at high temperatures, and (2) higher energy levels get more populated at higher temperatures, so that the spectra may get more crowded with hot bands and high J-number lines, especially when a multicomponent gas mixture is being studied. As will be reviewed in the following, many efforts have been devoted to reducing a correct absorption-free background and discriminate the molecular absorption by target species from a medley of various cross interference and noise processes.

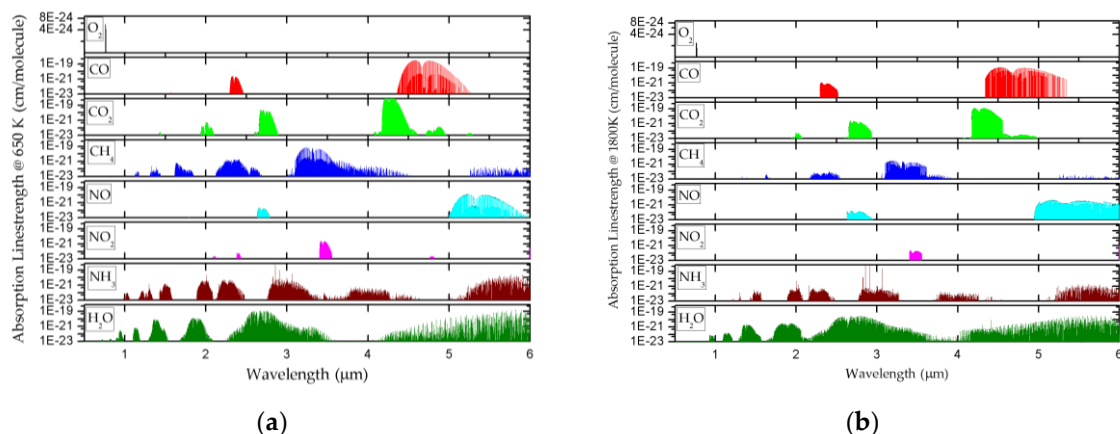


Figure 3. Absorption linestrengths for O_2 , CO, CO_2 , CH_4 , NO, NO_2 , NH_3 , and H_2O at (a) 650 K, (b) 1800 K. Transitions with line strengths less than 1×10^{-23} cm/molecule are not shown. All data taken from HITRAN2016 [47].

3. Fundamentals of Different LAS Measurement Schemes

Absorption is based on signal difference between the light intensities before and after propagation through a medium. When the incident light source has a spectral linewidth much narrower than the absorption transition feature, the so-gained spectral information can be regarded as single-wavelength without the need for light dispersion elements which can potentially introduce a reduction in spectral resolution. The use of semiconductor lasers which can be easily and fast tuned with injection current and temperature also allows the access to a range of wavelengths and absorption feature profiles with a single laser device. A detailed description of typical laser sources employed in LAS including distributed feedback lasers (DFBs), vertical-cavity surface-emitting lasers (VCSELs), Fourier-domain mode-locked lasers (FDML), quantum cascade lasers (QCLs), interband cascade lasers (ICLs), and their corresponding features, such as linewidth, power, and tunability has been presented by Goldenstein et al. [12] and Liu et al. [13].

The two most commonly employed schemes in realizing a LAS sensor with wavelength-tunable, narrow-linewidth lasers include direct absorption spectroscopy (DAS) and wavelength modulation spectroscopy (WMS), and each can be further associated with fixed- or scanned-wavelength schemes.

For fixed-wavelength DAS, as the laser wavelength is not tuned or modulated, the detection bandwidth is solely limited by the detector bandwidth and the sampling rate of the data acquisition system. Therefore, this scheme is often used in applications where an extremely high temporal resolution at levels of 1 MHz or above is needed. However, it requires the absolute laser wavelength to be accurately known and precisely controlled. In contrast, the scanned-wavelength scheme is widely used for its higher robustness and better immunity against fluctuations in practical combustion system monitoring.

The basic principles of DAS and WMS have been detailed elsewhere [48]. Here, from a different perspective, we will give a brief summary of each technique and elucidate the fitting algorithms used to infer gas conditions.

3.1. Direct Absorption Spectroscopy

The direct absorption method infers gas properties directly from the fractional transmission of light I_t/I_0 using the Beer–Lambert relation. One of the key problems to solve in DAS is thus to determine the baseline, i.e., the light intensity I_0 before absorption by the medium. Certain sensor systems incorporate an additional reference signal with a non-resonant laser or a broadly tunable light source to correct for the baseline [12]. However, this is at the expense of added components and may introduce potential errors from additional optical etalons. The more commonly adopted approach is to mathematically fit the baseline using non-absorbing portions within a scan.

Two background correction strategies are often adopted, namely, the Levenberg–Marquardt (LM) fitting algorithm [49–51], and the advanced integrative (AI) fitting algorithm [52]. Both fitting algorithms involve an iterative process, and the major difference lies in the fitting speed and multi-line fitting capability. More details are summarized in Table 1 below, and here we illustrate a typical fitting procedure with an example of AI fitting algorithm.

AI fitting process:

Step 1: Background correction: a polynomial fit is applied to infer the background from the non-absorbing portions;

Step 2: Retrieval of line center position ν_0 , which is estimated from the two symmetrical intervals from the maximum of background-corrected absorbance curve, thus no explicit initialization is needed;

Step 3: Retrieval of absorbance area: absorption linewidth is predetermined, and then the Voigt function is calculated;

Step 4: Voigt fit: several numerical approaches can be used to approximate the Voigt function [53,54] as no analytical form is available.

Most commonly, by using a low-order (order two to four) polynomial to fit the baseline and subsequently fitting the absorbance curve with a Voigt profile through an iterative process, the gas properties can be inferred. This works well for isolated or slightly overlapped features and if the baseline is reasonably smooth and the raw spectrum has a good SNR. However, when noises from harsh environments causing severe beam steering and baseline fluctuation carry frequency components comparable to the scanning/detection bandwidth, uncertainties in the DAS detection will significantly grow. Efforts to deal with such background drift will be detailed in Section 4.

Table 1. Comparison of fitting algorithms in direct absorption spectroscopy (DAS) and wavelength modulation spectroscopy (WMS) techniques. LM: Levenberg–Marquardt, AI: advanced integrative, SNR: signal-to-noise-ratio.

Technique	Parameter Initialization	Parameter Predetermined	Feature/Limitation
DAS LM algorithm	ν_0, T, X	no	Easy to fit multiple absorption lines
DAS AI algorithm	no	$\Delta\nu$	Complicated to fit multiple absorption lines, a factor of 3-4 faster than the LM algorithm
2f-WMS	T, X	P HITRAN/HITEMP database [47]	Calibrated on the basis of database, hard to calculate absolute T
Calibration-free WMS-2f/1f with fixed-wavelength laser characterization	ν_0, T, X	$i_1, i_2, \varphi_1, \varphi_2$ HITRAN/HITEMP database	Wavelength-dependent laser characteristics may lead to measurement errors
Calibration-free WMS-2f/1f with scanned-wavelength laser characterization	ν_0, T, X	$\nu(t), M_{I_0}(t)$ HITRAN/HITEMP database	Non-linear laser intensity variation along measurement beam path difficult to quantify
Recovery of DAS lineshapes	ν_0, T, X	$\varphi_1, X_{nf}, Y_{nf}$	Higher-order harmonics come with low SNR
DAS-calibrated WMS	no	P, T	Direct, on-the-fly calibration, increased precision and SNR for trace gas detection

3.2. 2f-WMS Method

By adding a high-frequency modulation to the laser injection current, the WMS scheme raises the signal detection band to a designated frequency range and later extracts the signal with band-pass filtering processes. This allows the method to have better noise rejection capability, and a 2~100 improvement in SNR has been demonstrated over DAS [55].

When the absorption features introduce distortions to the sinusoidally modulated laser intensity, harmonic components at integer multiples of the modulation frequency would appear. Due to the symmetry of an absorption feature about its line center, even orders of harmonic signals would peak near the line center position. For small modulation depths, the nonlinear laser intensity modulation can be neglected, and the peak of the second harmonic signal, or the 2f peak height, is a function of species concentration, pressure, and temperature and therefore can be taken as the target signal to measure [56,57]. The dependence on multiple non-precalibrated parameters is the major limitation of 2f-WMS method, however, for two-line thermometry, the 2f peak height ratio of the two selected lines can be directly reduced to linestrength ratio with the use of suitable modulation depth and line pair. Figure 4 shows the flow chart of the fitting procedure of the 2f-WMS method, including 2f peak ratio thermometry and species concentration extraction. To account for the unknown proportionality to environmentally dependent factors such as transmission losses and instantaneous laser intensity, the 2f peak magnitudes need to be pre-calibrated on the basis of HITRAN/HITEMP database line parameters with known pressure and temperature conditions and a nominal value of gas concentration.

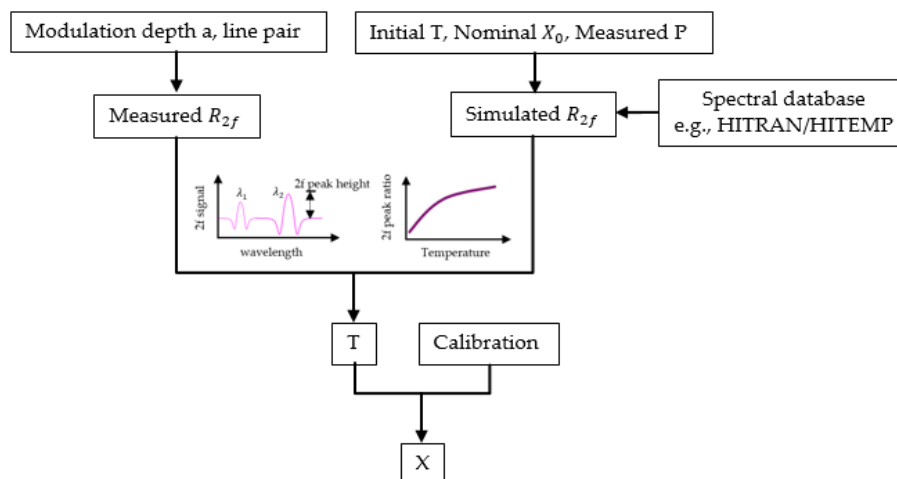


Figure 4. Flowchart of the $2f$ -WMS method.

3.3. Calibration-Free WMS- $2f/1f$ Method

The calibration process needed for the WMS- $2f$ method requires all environmental conditions to remain the same between the calibration stage and the actual measurement stage. Apparently, this luxury of having stable and known conditions is not always available, especially in practical applications where laser transmission fluctuations are much more difficult to predict or monitor. One solution is to normalize the $2f$ signal with the $1f$ component, referred to as the calibration-free WMS- $2f/1f$ method.

The normalization process cancels out the unknown or changing laser intensity. However, to directly associate the measured WMS- $2f/1f$ value with absolute gas conditions, laser intensity and frequency tuning parameters need to be accurately characterized. Typically, this laser characterization process identifies the first- and second-order laser intensity modulation indices (i_1, i_2) and intensity–frequency modulation phase shifts (φ_1, φ_2) at a specific center frequency ν_0 , which are sufficient to describe the intensity and frequency modulation behavior of a DFB semiconductor laser.

Rieker et al. summarized potential sources of uncertainty in calibration-free WMS, with particular emphasis on the influence of pressure and optical depth in harsh environments [55]. Under such conditions, measurement uncertainties induced by pressure deviation between the simulation and the experimental conditions become more significant, and preference for stronger absorption features voids the optical-thin assumption so that larger measurement errors may result.

In view of such problems, scanned-wavelength WMS with larger scan ranges and modulation depths may be used. A modified calibration-free WMS scheme with an entirely different laser characterization strategy is proposed to account for the time-variant and wavelength-dependent change of the laser characteristic parameters [16,58,59]. The flow chart of this method is shown in Figure 5. This analysis scheme differs from previous WMS strategies in two apparent ways: (1) the use of measured intensity in real time avoids the need for a pre-determined analytic model to describe laser intensity, and can at the same time account for the wavelength-dependent transmission of optical components in the beam path, and (2) using the same data processing procedure for both simulation and measurement introduces equal contributions from any potential non-ideal performance of the lock-in and low-pass filter.

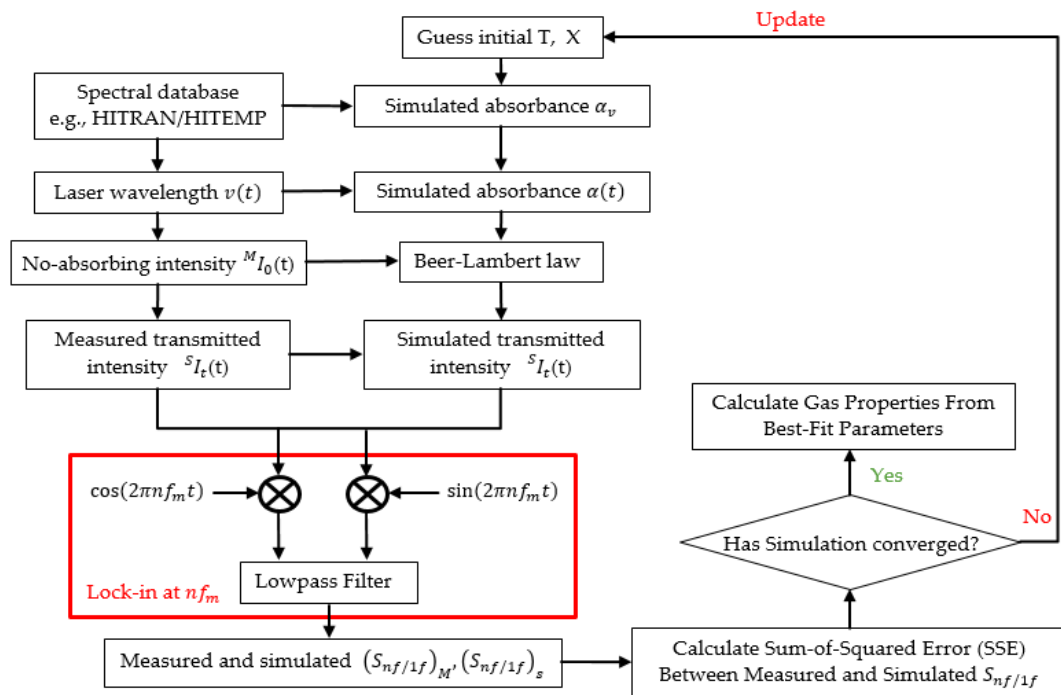


Figure 5. Flow chart of a calibration-free WMS scheme with scanned-wavelength laser characterization.

This method is applicable without constraints on optical depth or modulation index, so that pressure-broadened and blended absorption features can also be studied. However, nonlinear variations in laser characteristics due to calibration drift, temperature variations, and laser aging that add to the residual amplitude modulation (RAM) at different harmonic orders may introduce errors that mostly occur over longer terms.

3.4. Recovery of the Absorbance Profile Based On Higher-Order Harmonic Signals

While previous WMS approaches use the harmonic signals directly, a phasor decomposition method has been proposed to recover the absorbance profile from the first harmonic on the basis of RAM [60,61]. However, these earlier attempts only worked well with small modulation indices ($m < 0.2$) when the first-order harmonic shape is close to the first derivative of the absorbance profile. Peng et al. employed additional higher odd harmonics (3rd, 5th, . . .) to enhance the recovery accuracy with large modulation indices [62]. Figure 6 shows the flow chart of the recovery and data reduction process. It is worth noting that while considering more harmonic components improves the model recovery accuracy, these high-order terms usually have low SNRs and are difficult to detect in practical measurements.

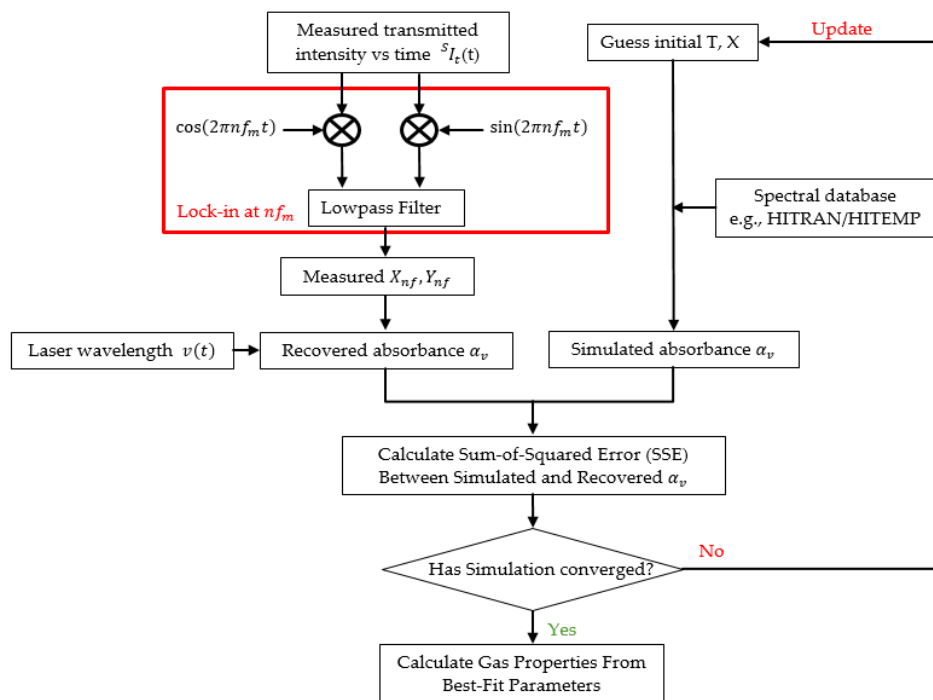


Figure 6. Flow chart of the recovery process of the absorbance profile based on higher-order harmonic signals.

3.5. DAS-Calibrated WMS

From the discussion above, one may conclude that DAS and WMS have their own advantages and limitations. While being more noise-immune in practical environments, calibration-free WMS methods rely on extensive laser characterization, and the nonlinear response to the sinusoidal modulation over the entire wavelength scan could lead to significant distortion in the $2f$ lineshape, especially with wide wavelength scans. Klein et al. have thus proposed a DAS-calibrated WMS method, which combines the simplicity and accuracy of the intrinsically calibration-free direct TDLAS (dTDLAS) with the enhanced precision of WMS- $2f$ [63]. A rapid (125 Hz) time-division multiplexed scheme alternating between triangular scan and scanned modulation was used to realize quasi-simultaneous DAS and WMS measurements. The concept of this on-the-fly calibration is illustrated in Figure 7. An absorbance level of 0.1 was chosen as the decision criterion of whether DAS only or DAS-calibrated WMS will be used. This largely extends the dynamic range of a single sensor and is especially advantageous for in-field measurements without the need for reference gases or measurement interruption.

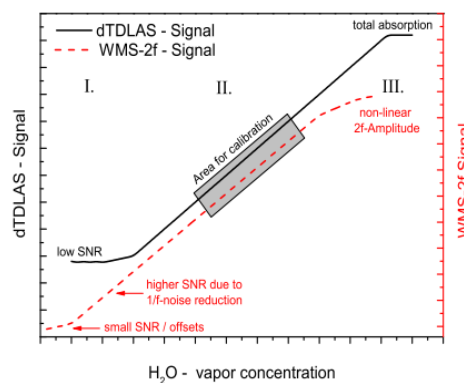


Figure 7. Schematic of the on-the-fly WMS calibration using time-multiplexed direct tunable diode laser absorption spectroscopy (dTDLAS) and WMS. Figure adapted from [63].

3.6. Summary of Measurement Schemes

A summary of various scanned-wavelength LAS techniques discussed above is presented in Table 1. For the purpose of comparison, fitting parameter initialization, parameter predetermination, as well as features and limitations for each algorithm are listed.

DAS is preferred for its calibration-free detection capability and simplicity, for applications where relatively isolated transitions are used. However, laser intensity fluctuations, excess noises, and baseline fitting errors put limitations to the use of this method especially for difficult environments. Thus, DAS is the method of choice for measurements with transitions of sufficient linestrength and narrow linewidth to allow laser access with wavelength scanning.

By contrast, the WMS method is more promising for measurement systems with small absorbance, high pressure broadening, or blended absorption features precluding a straightforward determination of the non-absorbing baseline. With $1f$ normalization, the calibration-free WMS- $2f/1f$ method can account for variations in laser intensity such as non-absorption losses due to light scattering or beam steering. This makes it advantageous for measurements in harsh environments involving high pressures, high opacity, high emission levels, and high temperatures.

The accuracy of DAS lineshape recovery from harmonic signals is limited by the low-SNR high-order terms, making this method unsuitable for practical measurements. A time-division multiplexed spectroscopic scheme is applied by alternating laser modulation and allows the enhancement of precision and dynamic range. This is an attractive strategy for in-field trace gas measurements without any need for reference gases or measurement interruption.

The LAS techniques discussed above typically provide a path-averaged parameter measurement over the zone of interest. Parameters including temperature, concentration, etc., are inferred by fitting measured and simulated spectral profiles. On the other hand, strategies have been developed to identify non-uniform characteristics in practical environments that commonly result from heat transfer, flow mixing, and combustion.

Two types of approaches including single line-of-sight (LOS) absorption and tomography have been proposed and experimentally demonstrated for the measurement of non-uniform zones. The first approach is based on either the *a priori* temperature (concentration) distribution profile or the probability density function along the LOS, namely, profile fitting and temperature binning, respectively [64]. It depends on simultaneous measurements of multiple absorption transitions with different temperature dependence. Tomography, on the other hand, relies on multiple LOS measurements and computational reconstruction algorithms. It reduces the requirements for spatially continuous optical access in traditional planar imaging and exhibits great potential for harsh and even optically dense environments [65]. However, this may complicate the optical system design and data processing of the experimental results.

Improvement in laser source and tomographic algorithms will contribute to greater accuracy in the temperature and concentration distribution reconstruction, using either of the two approaches above. Rieker et al. have extended the single LOS technique from advanced and expensive diode lasers with much broader tuning range (up to $10\text{--}15\text{ cm}^{-1}$) to a dual-frequency comb spectrometer [66,67]. The temperature distribution reconstruction accuracies increase as more absorption lines are incorporated. In addition, the development of hyperspectral laser sources enables measurements of a large number of absorption transitions and thereby significantly reduces the number of projections [68,69]. A detailed summary of laser absorption tomography (LAT) algorithms has been given by Cai et al. [65].

4. Strategies for Noise Reduction and Design Optimization

4.1. Sources of Noise

For any sensing system, the noise and uncertainty in the obtained results need to be assessed to evaluate the performance of the sensor. High noise levels not only obscure the signal to be measured but also make the data reduction process difficult and time-consuming. In the following, we will

first discuss the several major sources of noise in a LAS system, including laser noise, detector noise, analogue-to-digital conversion (ADC) noise, optical noise, and environmental noise [70,71]. Then, different approaches for noise reduction and signal optimization will be reviewed to guide future design considerations.

4.1.1. Laser and Detector Noise

The laser and detector excess noise are both frequency-dependent and known to have a pink noise spectrum. They are known as $1/f$ noise and are usually the dominant noise component at low frequencies from 1 to 10 kHz. The detector shot noise and thermal noise, on the other hand, are independent of frequency and known to have a white noise spectrum. Table 2 gives a brief summary and comparison of the different laser and detector noises.

Table 2. Comparison of laser and detector noises.

Type of noise	Cause	Feature	Frequency Range
Laser excess noise	Intensity fluctuation	Frequency dependent	1–10 kHz
Detector thermal noise	Thermal agitation of the charge carriers	Frequency independent	0.1–140 kHz
Detector shot noise	Discrete nature of electric charge	Frequency independent	0.1–140 kHz
Detector excess noise	Intensity fluctuation	Frequency dependent	1–10 kHz

4.1.2. Quantization Noise and ADC Resolution

The demands for accuracy and precision in trace species detection present great challenges for DAS. Therefore, high-speed and high-resolution ADC is required to recover the analogue detector signal with low quantization noise and to reduce the laser relative intensity noise (RIN, same as excess noise) through fast sampling. The frequency filtering feature of WMS has been widely adopted as it could improve the SNR by modulating and demodulating the absorption signal at an elevated frequency band. On the other hand, Lins et al. pointed out that as long as RIN is the dominating noise, the requirements for ADC resolution in $2f$ -WMS and DAS setups are in fact similar [72]. As suggested by the simulation results, when the RIN is low and sufficient ADC resolution is provided, DAS can provide higher SNR than WMS. In this case, with the advances of modern electronics and digital signal processing, DAS can have more advantages over WMS [73].

4.1.3. Optical Interference Fringe Noise

In a multi-element optical system with coherent light source, many flat surfaces can lead to optical interference fringes, often referred to as optical etalons. These optical fringes often exhibit a free-spectral-range (FSR) comparable to the linewidth of the absorbing species, so that they are difficult to be distinguished from target absorption features.

Various means have been attempted to minimize the influence of optical etalons, including careful optical design [74–76], mechanical dithering of optics [77–79], balanced-ratio detection schemes [80,81], calibration-free WMS [82–84], and digital filtering techniques [85–89]. A summary of these approaches is given in Table 3 and briefly discussed in the following.

Table 3. Comparison of strategies to minimize interference fringe noise. AR: anti-reflective, EMD: empirical mode decomposition.

Strategy	Solutions	Feature
Optical design	Wedged or AR-coated windows; Optical isolators; Etalon immune distance	Difficult to minimize etalon in complex optical systems
Mechanical modulation	Dithering or rotating of mirrors; Brewster-plate spoiler	Increased system complexity; Limited detection bandwidth
Balanced detection schemes	Split laser beam into the sample beam and reference beam	Difficult to replicate all optical effects in reference path
WMS	Modulation index optimization; Use of higher harmonics	SNR sacrificed
Digital filtering technique	Wavelet transform; Kalman filtering; EMD	Increasing computation cost; Parameters need to be set carefully

Optical etalons essentially arise from the constructive and destructive interferences when light bounces back and forth between parallel surfaces, similar to the way optical cavity modes are formed. Optical designs to avoid etalons are therefore approaches to reduce reflections and to scramble these standing-wave modes. This includes using wedged or anti-reflective (AR) -coated windows, optical isolators, and placing the optical elements at “etalon-immune distances” to avoid etalon effects from optical feedback. Collimated laser beams can be intentionally diverged before passing through optical thins and re-collimated thereafter. In addition to these passive optical designs, an active control of the optical system can be applied to effectively reduce etalons. Mechanical modulations, such as dithering or rotation of the mirrors and use of a Brewster-plate spoiler, are active control approaches taken in high-performance optical systems. However, these do largely increase the system’s cost and complexity and may limit the achievable detection bandwidth.

Certain laser devices exhibit unsuppressed cavity mode noise or fiber-coupling noise due to imperfect optical isolation, which appear as etalons on the output scans. Balanced-ratio detection schemes, also known as common-mode rejection schemes, are commonly employed to reduce such optical fringes. The laser beam is split into a measurement and a reference beam, and signals from the two detectors are fed into a balanced-ratio detection circuit that automatically cancels out the noises commonly present in the two signals. Etalons originated from the optical path external to the laser cannot generally be canceled in this way, since it would be difficult to achieve exactly the same beam path other than the portion being absorbed.

Etalon fringes often appear as low-frequency noises and can therefore be suppressed through the band-pass filtering process of WMS. On the other hand, fringe noises may add to the RAM and put additional constraint on selecting the optimal modulation parameters. This can lead to reduced SNR and larger uncertainties, especially since the optical alignment and etalon fringe profiles may change over time.

Digital filtering techniques are extensively investigated in absorption signal processing, including wavelet transform, Kalman filter, and empirical mode decomposition (EMD). These methods are purely from a standpoint of digital signal processing and frequency-domain analysis, thus require no additional optical or mechanical components. However, these techniques will inevitably increase the computation complexity, and the filter parameters need to be carefully designed on the basis of an appropriate understanding of the signal and noise characteristics. The extent of improvement that such techniques can achieve is ultimately limited by the quality of the light signal measured, so it is still of utmost importance to devote the best effort in designing a better optical system.

4.2. Strategies Based On Laser Control Parameter Optimization

The absorption signal can be enhanced by optimizing a number of laser control parameters including scanning amplitude, scan rate, modulation depth and frequency, and time delay constant of the lock-in amplifier.

A number of researchers have discussed parameter selection criteria for the WMS system. Werle et al. conducted a comprehensive analysis of the modulation degree so as to obtain maximum signal amplitude [8]; a Fourier series was utilized by Uehara et al. to analyze the relationship between modulated signals and optical penetration depth in frequency modulation [90]; Kluczyrski et al. theoretically studied the effect of modulation frequency [91]; Neethu et al. studied the optimization of a number of modulation parameters in realizing a LAS oxygen sensing system [92].

Table 4 summaries the effect of different control parameters on the $2f$ -signal waveforms including maximum amplitude, SNR, peak width, and peak height ratio (PHR).

Table 4. Effects of different control parameters on $2f$ signals. PHR: peak height ratio.

	Scanning Amplitude	Scanning Frequency	Modulation Depth	Modulation Frequency	Time Constant
Maximum $2f$	- ¹	↓ ³	↑↓	↑↓	↓
SNR	-	↑ or ↓	↑↓	↓	-
Peak width	↑ ²	↑	-	↓	-
PHR	↑	↓	-	↑ or - ⁴	-

¹ no evident correlation, ² increase, ³ decrease, ⁴ unchanged.

Due to the complex intercorrelation between various laser characteristic parameters, no explicit mathematical expressions generally exist to describe the dependence of the WMS signal on the laser control parameters. Therefore, the selection and optimization of these control parameters usually rely on empirical attempts and maximization of the target signal. The laser scan range, for example, is simply set to cover the target absorption feature and just enough non-absorption portions for baseline fitting, without leaving excessive margin which will decrease the detection bandwidth. For WMS in general, the modulation depth is chosen so that the WMS- $2f$ signal at absorption line center is maximized. It has been demonstrated that for an isolated absorption feature, the highest peak value can be achieved by selecting the modulation depth to be 1.1 times the full-width-at-half-maximum (FWHM) $\Delta\nu$ of the absorption feature [55].

In conventional scanned-wavelength WMS, a high-frequency sinusoidal wave is superimposed on a linear ramp of the laser injection current. As the laser tuning function can now readily be controlled digitally, variation of this tuning waveform can bring increased flexibility to signal optimization. Fried et al. employed a jump scanning function and dual fitting analysis to simultaneously optimize signals from two selected absorption profiles [93]. Chen et al. modified the linear ramp function so that the laser scanned more slowly near the line center ([94], Figure 8). The scan portion with stronger absorption thus occupied a larger fraction of the scan, resulting in the improvement of the overall SNR. Consequently, a factor of 1.8 improvement was observed with $2f$ detection, and an even higher enhancement by a factor of 3.3 was obtained with direct absorption measurements.

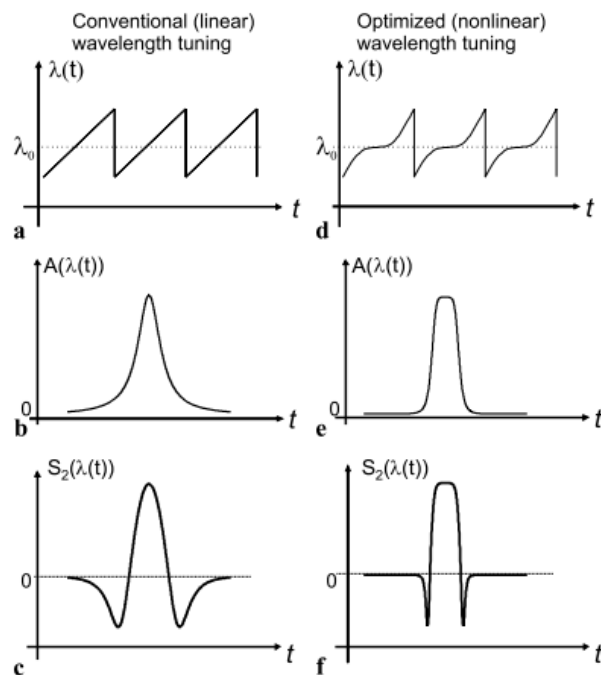


Figure 8. Schematic illustration of the wavelength scanning function: conventional (linear) (a) and optimized (nonlinear) (d). The resulting spectrum waveform is shown for direct spectroscopy in (b) for linear scanning and (e) for nonlinear scanning as well as for WMS (second harmonic detection) in (c,f). Figure adapted from [94].

When multi-species detection is attempted by using closely spaced absorption lines accessible with a single laser scan, the different widths and line profiles of the target species may impose significantly different optimization targets according to the optimal modulation depth criteria stated above. Du et al. demonstrated an *in situ*, multi-parameter LAS sensor during a selective catalytic reduction (SCR) process by accessing four H₂O spectral transitions and a group of NH₃ lines with a single diode laser [95]. As can be seen in Figure 9, WMS with varied modulation amplitude (WMS-VMA) and an optimized multispectral fitting algorithm was used to satisfy the optimization targets for both the H₂O and the NH₃ lines.

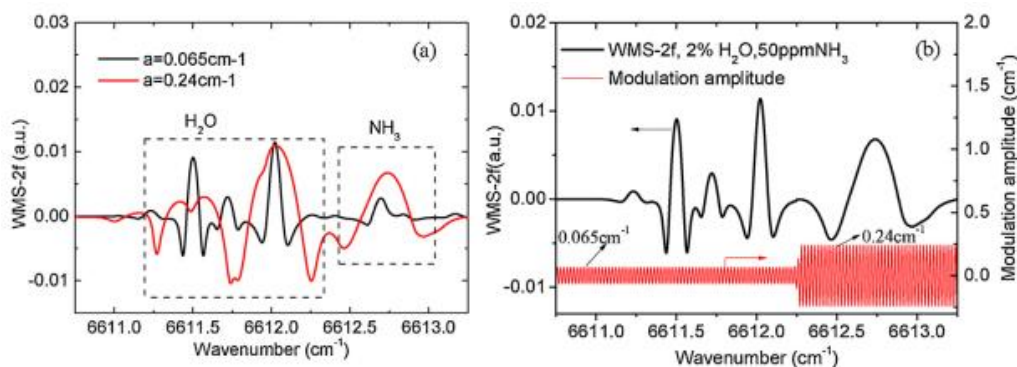


Figure 9. Simulated WMS-2f signal with (a) modulation amplitude 0.065 cm⁻¹ and 0.24 cm⁻¹, respectively; (b) wavelength modulation spectroscopy with varied modulation amplitude (WMS-VMA). Figure adapted from [95].

WMS-2f detection is sensitive to the curvature of the signal. When blending different spectral features becomes more significant, absorption from the wings of adjacent lines would alter the curvature at the target line center, so that maximizing the line center 2f magnitude of an individual transition

no longer renders the optimum of overall signal. In such cases, the optimal modulation depth a_m may largely deviate from the theoretical value of $\sim 1.1 \Delta\nu$. Peng et al. proposed a novel procedure for choosing an optimal WMS modulation depth in the presence of spectral interference by defining a new figure of merit to account for the spectral interference [96,97].

As shown in Equations (2) and (3), F and σ are defined to quantify the inverse magnitude of the WMS-2f signal and the sensitivity to spectral interference, respectively:

$$F(a_m) = \frac{S_{2f, max}}{S_{2f}(a_m)} \quad (2)$$

$$\sigma(a_m) = \left| \frac{S_{2f/1f, intf}(a_m, \bar{\phi}) - S_{2f/1f}(a_m)}{S_{2f/1f}(a_m)} \right| \quad (3)$$

where S_{2f} is the total interference-free WMS-2f signal at the target transition line center, $S_{2f, max}$ is the maximum possible interference-free WMS-2f signal, and $S_{2f/1f}$ is the WMS-2f/1f.

Ideally, a_m should be chosen so that both the inverse signal magnitude F and the perturbation from interference σ are simultaneously minimized. Such an a_m does not generally exist, so the strategy is to select $a_{m, opt} = \text{argmin}(C)$, where the cost function $C = \sigma F$ is now the target of optimization. The so-obtained optimal modulation depth $a_{m, opt}$ is indicated by the black dashed line in Figure 10 at the minimum of C , where the value of F at this modulation depth is 1.5, indicating that 33% of the potential SNR is sacrificed.

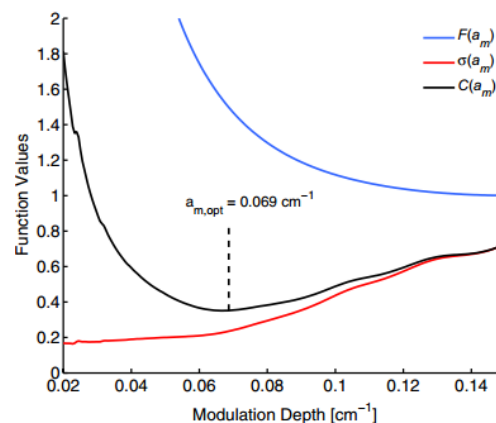


Figure 10. Inverse WMS-2f signal strength (F , blue line), NH_3 interference sensitivity (σ , red line), and cost function (C , red line) vs modulation depth for a 3 ppm NH_3 mixture in CH_4 – air $\phi = 0.6$ combustion exhaust at $T = 600 \text{ K}$, $P = 1 \text{ atm}$. The optimal modulation depth $a_{m, opt}$ is shown in the black/dashed line. Figure adapted from [96].

4.3. Strategies based On Signal Processing Schemes

4.3.1. Baseline Fitting for Blended Absorption Feature

As discussed above, using the AI or LM fitting algorithms to calculate the laser intensity baseline requires proper identification of the absorption-free flanks. However, for spectra with low SNR, distinguishing the non-absorption area using direct visual inspection (DVI) is hard. A new strategy was proposed by Li et al. using wavelet decomposition and iteration to remove the background drift [98]. The application of wavelet transform (WT) for TDLAS signal denoising is based on finding the optimal wavelet pairs to determine the baseline. Figure 11 shows effective nonlinear baseline correction and denoising using discrete wavelet transform (DWT). Compared with the commonly used DVI method, this DWT algorithm demonstrated potential for batch processing of TDLAS spectra. However, system cost and complexity increased.

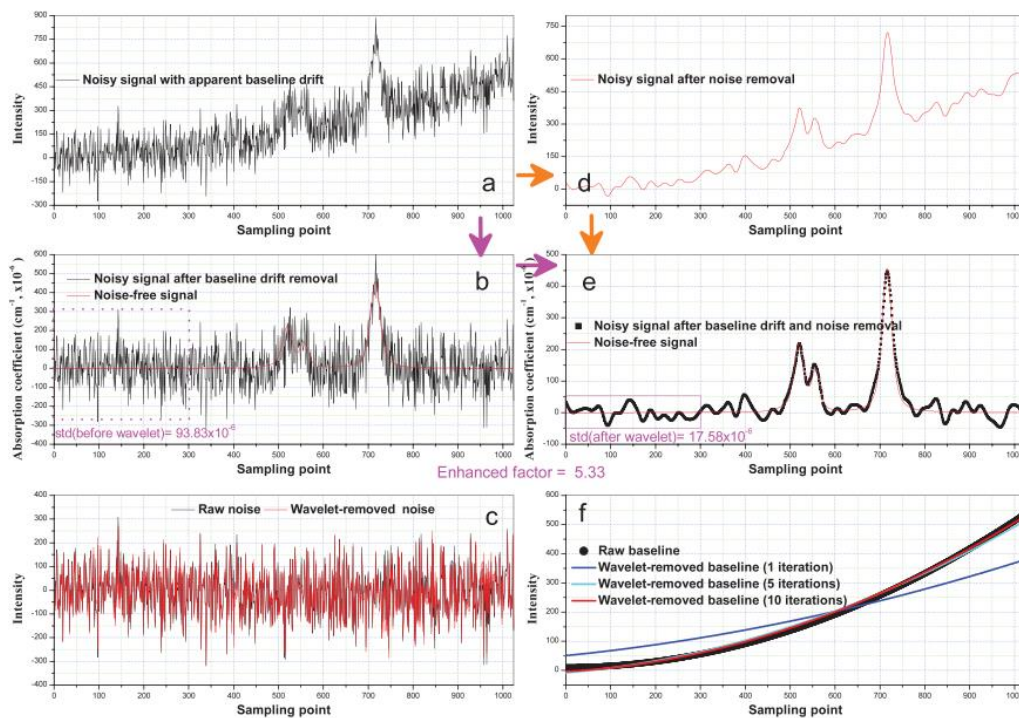


Figure 11. Nonlinear baseline correction and denoising using discrete wavelet transform (DWT). (a) Noisy signal with apparent baseline drift; (b) baseline drift-removed signal from (a) and noise-free signal; (c) raw noise and wavelet-removed noise; (d) denoised signal from (a); (e) baseline drift-removed signal from (d) and noise-free signal; (f) raw baseline and wavelet-removed baselines with different iterations. Figure adapted from [98].

Weisberger et al. have developed a blended-feature baseline fitting method (BFBL) using a more efficient iterative lookup table approach [99]. The baseline is estimated by coupling measured data with simulated fractional transmission at the peaks between absorption features known as baseline anchor points. Figure 12 illustrates the fitting procedure, and this technique was validated against measurements in a static heated cell and a wood-fired two-stage hydronic heater. The results indicated that it can be very useful with multiple overlapping absorption features.

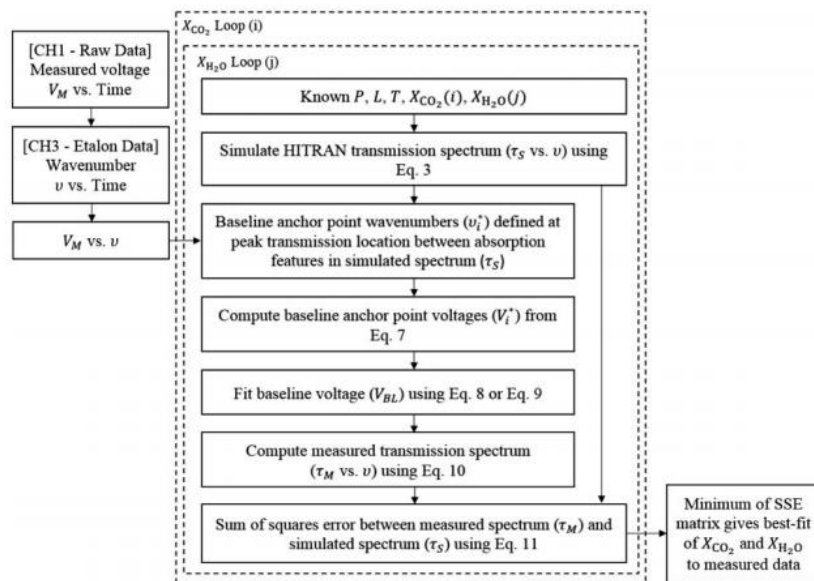


Figure 12. Flow chart for DAS baseline fitting data analysis. Figure adapted from [99].

4.3.2. In Situ Parameter Fitting

In Section 3, we have discussed the limitation of calibration-free WMS when it is important to perform accurate assessments of laser characteristics. It is often assumed that the magnitude of wavelength modulation is constant over the entire scanning range [58] and the differential current-to-wavelength tuning behavior is linear for small current variations around a bias point [100,101]. Such assumption may nevertheless introduce different degrees of uncertainty under different circumstances. Zhao et al. presented an improved methodology for assessing the wavelength response of a DFB laser by using a high-order empirical formula [102].

Although the laser characterization process is not difficult by itself, the task of accurately tracking its variations in real time is nontrivial. More recently, Upadhyay et al. have proposed a new calibration-free 2f-WMS technique to measure gas concentration and pressure without the need for laser pre-characterization [103–106]. Similar to the idea of DAS baseline fitting, the harmonic backgrounds, i.e., RAMs, are obtained by interpolating the non-absorbing wings of the X and Y components of the demodulated 1f, 2f, and 3f signals (Figure 13). The intensity modulation indices i_n can then be obtained from the RAMs, whereas the intensity–frequency modulation phase shifts φ_n can be obtained by taking the inverse tangent of the ratio of X and Ys.

The *in situ* and real-time characterization of relevant laser parameters ensures that the measurements are not affected by rapid non-absorbing laser intensity variations such as those due to light scattering, beam steering, vibrations, and window fouling or by slow variation effects such as temperature changes, calibration drift, and aging of the devices. However, even if it has been demonstrated that higher-order harmonic signals would have reduced spectral interference from neighboring lines, the requirement for non-absorbing baseline portions for the fitting still puts limitations to the applicable scope of this method.

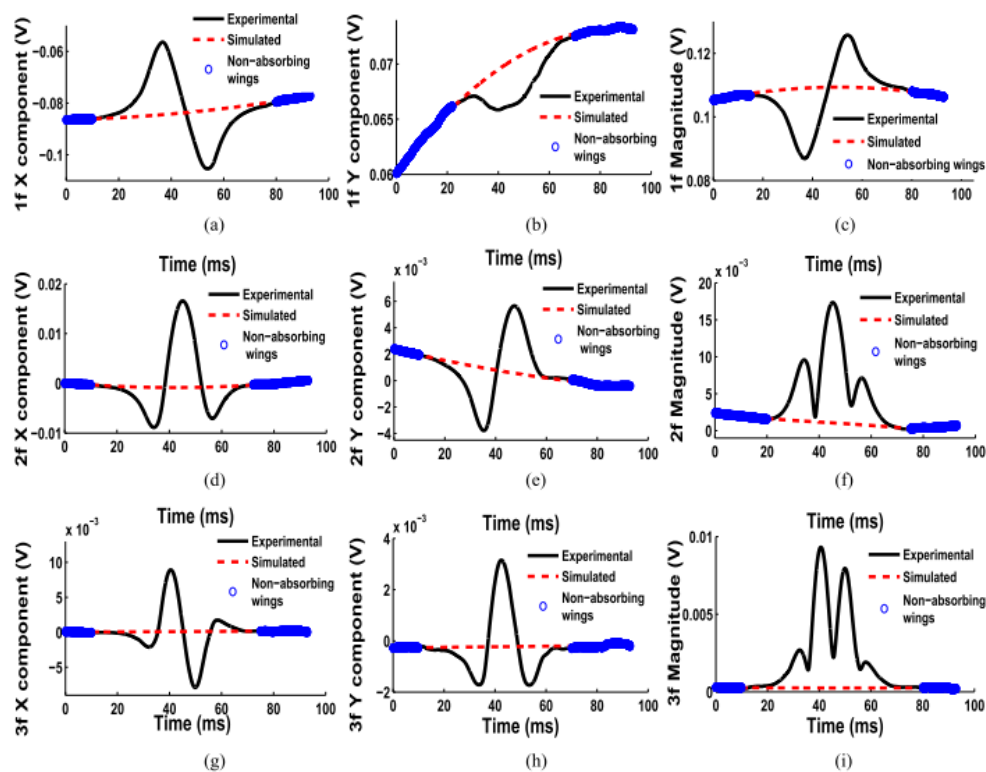


Figure 13. The 1650 nm DFB laser was modulated at $m = 2.2$, and the transmitted light through a 1% CH₄ sample at 1 bar pressure was demodulated by a lock-in amplifier (LIA) to obtain (a) 1f X-component along $I H_1$, (b) 1f Y-component orthogonal to $I H_1$, (c) magnitude of 1f Signal, (d) 2f X-component along $I H_2$, (e) 2f Y-component orthogonal to $I H_2$, (f) magnitude of 2f Signal, (g) 3f X-component along $I H_3$, (h) 3f Y-component orthogonal to $I H_3$, and (i) magnitude of 3f Signal. Figure adapted from [104].

4.3.3. Harmonic Wavelet Analysis of Modulated TDLAS Signals

Calibration-free WMS is essentially a signal processing technique to extract information about molecular absorption from a noisy environment with higher signal fidelity. In view of the unsolved issues arising from potential uncertainties in laser characteristic parameters, spectroscopic constants, as well as requirements for digital filter design in the digital lock-in amplification process [107–109], new signal analysis methodologies have been proposed to better analyze the time-dependent signal harmonics.

Duan et al. have employed signal processing techniques based on wavelet analysis of modulated signals obtained from TDLAS and demonstrated that wavelets have the potential to enable the detection of signal harmonics [110]. In addition to a pure frequency domain analysis, windowed Fourier analysis can provide information on the time dependence of the frequency components but will suffer from substantial inaccuracy when the window width decreases. As an alternative, wavelet analyses can provide more accurate information on this time-dependent evolution of different frequency components and have become popular in recent years.

Figure 14 shows the comparison of wavelet analyses of level 8, 9, and 10 with analytical predictions from a Voigt absorption profile. Each level corresponds to a specific value related to scaling in DWT. As the level increases, the frequency resolution of the wavelet analysis increases. With the shown correlation between the two, it is apparent that wavelet analysis performed well in extracting the $1f$ and $2f$ harmonics. This work demonstrated the potential of wavelet analyses in yielding a new methodology for the improvement of the conventional TDLAS system.

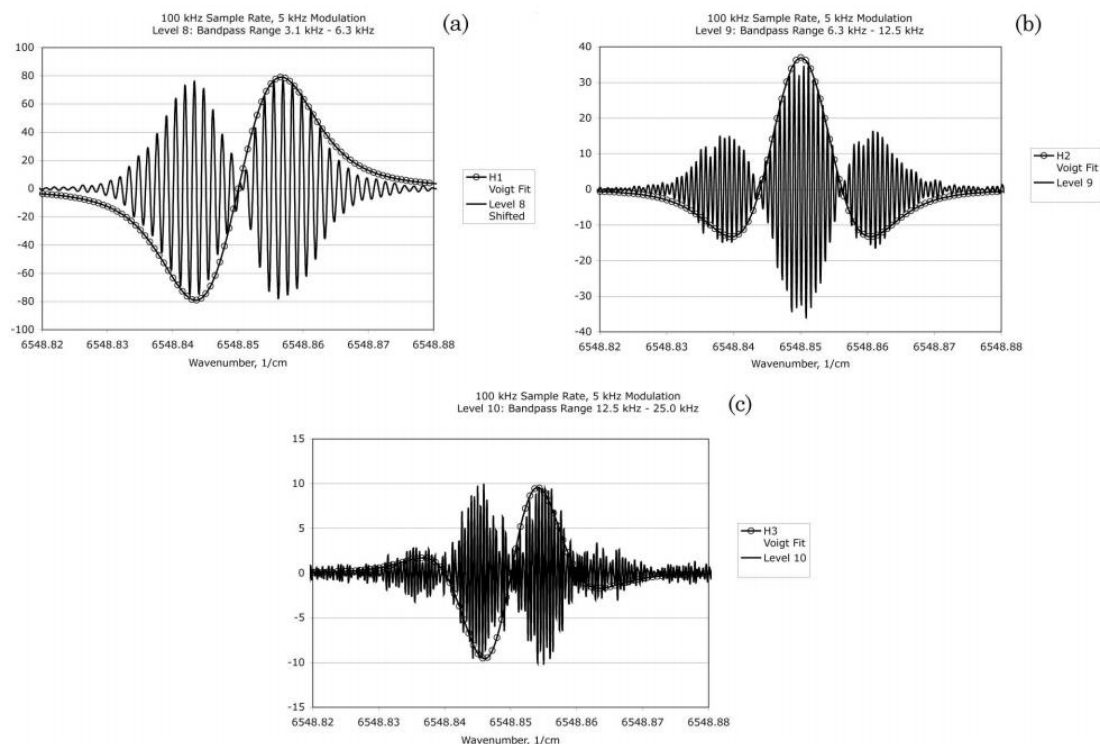


Figure 14. Comparison of results from the wavelet analyses with (a) H_1 , (b) H_2 , and (c) H_3 coefficients obtained with a Voigt absorption profile. Figure adapted from [110].

5. Conclusions and Future Outlook

Efforts in improving LAS sensor performance suitable for practical environments have never stopped attracting the attention of researchers and developers. By overviewing the achievements of the developed sensors, particularly with sensor deployment in laboratory studies, industrial processes, and engine diagnostics, it can be understood that different measurement applications pose largely different demands in terms of detection limits and bandwidths. In this review, we have

attempted to establish a logical development from a system design perspective, for the purpose of better understanding measurement needs and providing guidelines and insights for designing a laser absorption sensing system. Understanding the different sources and processes of noise is the prerequisite for proposing appropriate strategies for SNR amelioration. Under typical measurement conditions, analogue and digital noise from opto-electronic devices, optical noise from the optical system, and excess noise from the environment are the most relevant disturbances that contribute to signal deterioration. In addition to designing a better optical system, strategies of noise reduction and design optimization play important roles in improving a sensor performance and achieving better adaptation to various environments. This can be done through either optimization of laser control and tuning parameters or various algorithms for data processing, such as baseline extraction, *in situ* laser characterization, and wavelet analysis. It is realized that the need for sensing technology development is highly fragmented and demand-driven. While each measurement strategy has its limitations and constraints in face of the challenges from complex environments, much needs to be done from an engineering design perspective and to profoundly comprehend the underlying scientific fundamentals in terms of optics, spectroscopy, and signal processing.

Author Contributions: Z.W. collected references, drafted and revised the paper; P.F. collected references and revised the paper; X.C. supervised the whole work, designed the paper and revised the draft.

Funding: This material is based on work supported by the National Science Foundation of China under Grant No. 51606111 and No. 61627804.

Conflicts of Interest: The author declares no conflict of interest.

Nomenclature

LAS	Laser absorption spectroscopy
DAS	Diode absorption spectroscopy
WMS	Wavelength modulation spectroscopy
TDLAS	Tunable diode laser absorption spectroscopy
LOS	Line-of-sight
SNR	Signal-to-noise ratio
I_t [W/cm ²]	Transmitted light intensity
I_0 [W/cm ²]	Incident light intensity
α_ν	Absorbance
k_ν [1/cm]	Spectral absorption coefficient
L [cm]	Absorption pathlength
n [molecule/cm ³]	Number density of the absorbing species
σ_ν [cm ² /molecule]	Absorption cross-section
S [cm ⁻² /atm]	Absorption linestrength
ϕ_ν [cm]	Frequency-dependent lineshape function
P [atm]	Pressure
X_i	Mole fraction of the absorbing species i
ν	Light frequency
NEA	Noise equivalent absorbance
DFBs	Distributed feedback lasers
VCSELS	Vertical-cavity surface-emitting lasers
FDML	Fourier-domain mode locked
QCLs	Quantum cascade lasers
ICLs	Interband cascade lasers
LM	Levenberg–Marquardt
AI	Advanced integrative
HITRAN	High Resolution Transmission
HITEMP	High Temperature
R_{2f}	$2f$ peak ratio
T	Temperature

X_0	Nominal concentration
a	Modulation depth
$i_1,$	1st-order laser intensity modulation indices
i_2	2nd-order laser intensity modulation indices
φ_1	1st-order laser intensity–frequency modulation phase shifts
φ_2	2nd-order laser intensity–frequency modulation phase shifts
ν_0	Specific center frequency
$\nu(t)$	Laser wavelength
$\alpha(t)$	Simulated absorbance
$^M I_0(t)$	No-absorbing intensity
$^S I_t(t)$	Measured transmitted intensity
$^S I_t(t)$	Simulated transmitted intensity
f_m	Modulation frequency
m	Modulation index
$(S_{nf/1f})_M$	Measured 1f-normalized nf signal
$(S_{nf/1f})_S$	Simulated 1f-normalized nf signal
SSE	Sum-of-squared error
RAM	Residual amplitude modulation
X_{nf}	Measured X component of nf signal
Y_{nf}	Measured Y component of nf signal
LAT	Laser absorption tomography
ADC	Analogue-to-digital conversion
RIN	Relative intensity noise
EMD	Empirical mode decomposition
PHR	Peak height ratio
$\Delta\nu$	Full-width-at-half-maximum
FWHM	Full-width-at-half-maximum
SCR	Selective catalytic reduction
WMS-VMA	Wavelength modulation spectroscopy with varied modulation amplitude
a_m	Modulation depth
F	Inverse WMS-2f signal strength
σ	Interference sensitivity
C	Cost function
S_{2f}	Interference-free WMS-2f signal at the target transition line center
$S_{2f, max}$	Maximum possible interference-free WMS-2f signal
$a_{m, opt}$	Optimal modulation depth
DVI	Direct visual inspection
WT	Wavelet transform
DWT	Discrete wavelet transform
BFBL	Blended-feature baseline fitting method
i_n	n^{th} -order laser intensity modulation indices
φ_n	n^{th} -order laser intensity–frequency modulation phase shifts
LIA	Lock-in amplifier

References

1. Hanson, R.K.; Falcone, P.K. Temperature measurement technique for high temperature gases using a tunable diode laser. *Appl. Opt.* **1978**, *17*, 2477–2480. [[CrossRef](#)] [[PubMed](#)]
2. Ried, J.; Shewchun, J.; Garside, B.K.; Balik, E.A. High sensitivity pollution detection employing tunable diode lasers. *Appl. Opt.* **1978**, *17*, 300–307. [[CrossRef](#)] [[PubMed](#)]
3. Druy, M.A. From laboratory technique to process gas sensor: The maturation of tunable diode laser absorption spectroscopy. *Spectroscopy* **2006**, *21*, 14–18.
4. Lackner, M. Tunable diode laser absorption spectroscopy in the process industries: A review. *Rev. Chem. Eng.* **2007**, *23*, 65–147. [[CrossRef](#)]

5. Available online: www.oxigraf.com (accessed on 3 July 2019).
6. Wolfrum, J. *Lasers in Combustion: From Basic Theory to Practical Devices*; Elsevier: Amsterdam, The Netherlands, 1998; Volume 27, pp. 1–41.
7. Allen, M.G. Diode laser absorption sensors for gas-dynamic and combustion flows. *Meas. Sci. Technol.* **1998**, *9*, 545–562. [[CrossRef](#)] [[PubMed](#)]
8. Werle, P. A review of recent advances in semiconductor laser based gas monitors. *Spectrochim. Acta Part A Mol. Biomol. Spectrosc.* **1998**, *54*, 197–236. [[CrossRef](#)]
9. Nasim, H.; Jamil, Y. Recent advancements in spectroscopy using tunable diode lasers. *Laser Phys. Lett.* **2013**, *10*, 043001. [[CrossRef](#)]
10. Hanson, R.K. Applications of quantitative laser sensors to kinetics, propulsion and practical energy systems. *Proc. Combust. Inst.* **2011**, *33*, 1–40. [[CrossRef](#)]
11. Bolshov, M.A.; Kuritsyn, Y.A.; Romanovskii, Y.V. Tunable diode laser spectroscopy as a technique for combustion diagnostics. *Spectrochim. Acta Part B Atomic Spectrosc.* **2015**, *106*, 45–66. [[CrossRef](#)]
12. Goldenstein, C.S.; Spearrin, R.M.; Jeffries, J.B.; Hanson, R.K. Infrared laser-absorption sensing for combustion gases. *Prog. Energy Combust. Sci.* **2017**, *60*, 132–176. [[CrossRef](#)]
13. Liu, C.; Xu, L. Laser absorption spectroscopy for combustion diagnosis in reactive flows: A review. *Appl. Spectrosc. Rev.* **2018**, *54*, 1–44. [[CrossRef](#)]
14. Li, J.; Yu, B.; Zhao, W.; Chen, W. A review of signal enhancement and noise reduction techniques for tunable diode laser absorption spectroscopy. *Appl. Spectrosc. Rev.* **2014**, *49*, 666–691. [[CrossRef](#)]
15. Zhang, T.; Kang, J.; Meng, D.; Wang, H.; Mu, Z.; Zhou, M.; Chen, C. Mathematical Methods and Algorithms for Improving Near-Infrared Tunable Diode-Laser Absorption Spectroscopy. *Sensors* **2018**, *18*, 4295. [[CrossRef](#)] [[PubMed](#)]
16. Chao, X.; Jeffries, J.B.; Hanson, R., K. In situ absorption sensor for NO in combustion gases with a 5.2 μm quantum-cascade laser. *Proc. Combust. Inst.* **2011**, *33*, 725–733. [[CrossRef](#)]
17. Wagner, S.; Fisher, B.T.; Fleming, J.W.; Ebert, V. TDLAS-based in situ measurement of absolute acetylene concentrations in laminar 2D diffusion flames. *Proc. Combust. Inst.* **2009**, *32*, 839–846. [[CrossRef](#)]
18. Wagner, S.; Klein, M.; Kathrotia, T.; Riedel, U.; Dreizler, A.; Ebert, V. In situ TDLAS measurement of absolute acetylene concentration profiles in a non-premixed laminar counter-flow flame. *Appl. Phys. B* **2012**, *107*, 585–589. [[CrossRef](#)]
19. Nau, P.; Koppmann, J.; Lackner, A.; Kohse-Höinghaus, K.; Brockhinke, A. Quantum cascade laser-based MIR spectrometer for the determination of CO and CO₂ concentrations and temperature in flames. *Appl. Phys. B* **2015**, *118*, 361–368. [[CrossRef](#)]
20. Wagner, S.; Klein, M.; Kathrotia, T.; Riedel, U.; Kissel, T.; Dreizler, A.; Ebert, V. Absolute, spatially resolved, in situ CO profiles in atmospheric laminar counter-flow diffusion flames using 2.3 μm TDLAS. *Appl. Phys. B* **2012**, *109*, 533–540. [[CrossRef](#)]
21. Wunderle, K.; Wagner, S.; Pasti, I.; Pieruschka, R.; Rascher, U.; Schurr, U.; Ebert, V. Distributed feedback diode laser spectrometer at 2.7 μm for sensitive, spatially resolved H₂O vapor detection. *Appl. Opt.* **2009**, *48*, B172–B182. [[CrossRef](#)]
22. Seidel, A.; Wagner, S.; Dreizler, A.; Ebert, V. Robust, spatially scanning, open-path TDLAS hygrometer using retro-reflective foils for fast tomographic 2-D water vapor concentration field measurements. *Atmos. Meas. Tech.* **2015**, *8*, 2061–2068. [[CrossRef](#)]
23. Vanderover, J.; Wang, W.; Oehlschlaeger, M.A. A carbon monoxide and thermometry sensor based on mid-IR quantum-cascade laser wavelength-modulation absorption spectroscopy. *Appl. Phys. B* **2011**, *103*, 959–966. [[CrossRef](#)]
24. Stranic, I.; Hanson, R.K. Laser absorption diagnostic for measuring acetylene concentrations in shock tubes. *J. Quant. Spectrosc. Radiat. Transf.* **2014**, *142*, 58–65. [[CrossRef](#)]
25. Utsav, K.C.; Nasir, E.F.; Farooq, A. A mid-infrared absorption diagnostic for acetylene detection. *Appl. Phys. B* **2015**, *120*, 223–232.
26. Spearrin, R.M.; Li, S.; Davidson, D.F.; Jeffries, J.B.; Hanson, R.K. High-temperature iso-butene absorption diagnostic for shock tube kinetics using a pulsed quantum cascade laser near 11.3 μm . *Proc. Combust. Inst.* **2015**, *35*, 3645–3651. [[CrossRef](#)]

27. Sun, K.; Wang, S.; Sur, R.; Chao, X.; Jeffries, J.B.; Hanson, R.K. Sensitive and rapid laser diagnostic for shock tube kinetics studies using cavity-enhanced absorption spectroscopy. *Opt. Express* **2014**, *22*, 9291–9300. [[CrossRef](#)]
28. Sun, K.; Wang, S.; Sur, R.; Chao, X.; Jeffries, J.B.; Hanson, R.K. Time-resolved in situ detection of CO in a shock tube using cavity-enhanced absorption spectroscopy with a quantum-cascade laser near 4.6 μm . *Opt. Express* **2014**, *22*, 24559–24565. [[CrossRef](#)]
29. Ebert, V.; Fitzer, J.; Gerstenberg, I.; Pleban, K.U.; Pitz, H.; Wolfrum, J.; Jochem, M.; Martin, J. Simultaneous laser-based in situ detection of oxygen and water in a waste incinerator for active combustion control purposes. In Proceedings of the Symposium (International) on Combustion, Boulder, Colorado, USA, 2–7 August 1998.
30. Teichert, H.; Fernholz, T.; Ebert, V. Simultaneous in situ measurement of CO, H₂O, and gas temperatures in a full-sized coal-fired power plant by near-infrared diode lasers. *Appl. Opt.* **2003**, *42*, 2043–2051. [[CrossRef](#)] [[PubMed](#)]
31. Ebert, V.; Teichert, H.; Strauch, P.; Kolb, T.; Seifert, H.; Wolfrum, J. Sensitive in situ detection of CO and O₂ in a rotary kiln-based hazardous waste incinerator using 760 nm and new 2.3 μm diode lasers. *Proc. Combust. Inst.* **2005**, *30*, 1611–1618. [[CrossRef](#)]
32. Sun, K.; Sur, R.; Jeffries, J.B.; Hanson, R.K.; Clark, T.; Anthony, J.; Northington, J. Application of wavelength-scanned wavelength-modulation spectroscopy H₂O absorption measurements in an engineering-scale high-pressure coal gasifier. *Appl. Phys. B* **2014**, *117*, 411–421. [[CrossRef](#)]
33. Nau, P.; Kutne, P.; Eckel, G.; Meier, W.; Hotz, C.; Fleck, S. Infrared absorption spectrometer for the determination of temperature and species profiles in an entrained flow gasifier. *Appl. Opt.* **2017**, *56*, 2982–2990. [[CrossRef](#)]
34. Witzel, O.; Klein, A.; Wagner, S.; Meffert, C.; Schulz, C.; Ebert, V. High-speed tunable diode laser absorption spectroscopy for sampling-free in-cylinder water vapor concentration measurements in an optical IC engine. *Appl. Phys. B* **2012**, *109*, 521–532. [[CrossRef](#)]
35. Witzel, O.; Klein, A.; Meffert, C.; Wagner, S.; Kaiser, S.; Schulz, C.; Ebert, V. VCSEL-based, high-speed, in situ TDLAS for in-cylinder water vapor measurements in IC engines. *Opt. Express* **2013**, *21*, 19951–19965. [[CrossRef](#)] [[PubMed](#)]
36. Witzel, O.; Klein, A.; Meffert, C.; Schulz, C.; Kaiser, S.A.; Ebert, V. Calibration-free, high-speed, in-cylinder laser absorption sensor for cycle-resolved, absolute H₂O measurements in a production IC engine. *Proc. Combust. Inst.* **2015**, *35*, 3653–3661. [[CrossRef](#)]
37. Jatana, G.S.; Magee, M.; Fain, D.; Naik, S.V.; Shaver, G.M.; & Lucht, R.P. Simultaneous high-speed gas property measurements at the exhaust gas recirculation cooler exit and at the turbocharger inlet of a multicylinder diesel engine using diode-laser-absorption spectroscopy. *Appl. Opt.* **2015**, *54*, 1220–1231. [[CrossRef](#)] [[PubMed](#)]
38. Spearrin, R.M.; Goldenstein, C.S.; Schultz, I.A.; Jeffries, J.B.; Hanson, R.K. Simultaneous sensing of temperature, CO, and CO₂ in a scramjet combustor using quantum cascade laser absorption spectroscopy. *Appl. Phys. B* **2014**, *117*, 689–698. [[CrossRef](#)]
39. Schultz, I.A.; Goldenstein, C.S.; Strand, C.L.; Jeffries, J.B.; Hanson, R.K. Hypersonic scramjet testing via TDLAS measurements of temperature and column density in a reflected shock tunnel. In Proceedings of the 52nd Aerospace Sciences Meeting, National Harbor, MD, USA, 13–17 January 2014.
40. Caswell, A.W.; Roy, S.; An, X.; Sanders, S.T.; Schauer, F.R.; Gord, J.R. Measurements of multiple gas parameters in a pulsed-detonation combustor using time-division-multiplexed Fourier-domain mode-locked lasers. *Appl. Opt.* **2013**, *52*, 2893–2904. [[CrossRef](#)] [[PubMed](#)]
41. Caswell, A.; Roy, S.; An, X.; Sanders, S.; Hoke, J.; Schauer, F.; Gord, J. High-bandwidth H₂O absorption sensor for measuring pressure, enthalpy, and mass flux in a pulsed-detonation combustor. In Proceedings of the 50th AIAA Aerospace Sciences Meeting including the New Horizons Forum and Aerospace Exposition, Nashville, TN, USA, 9–12 January 2012.
42. Goldenstein, C.S.; Spearrin, R.M.; Jeffries, J.B.; Hanson, R.K. Infrared laser absorption sensors for multiple performance parameters in a detonation combustor. *Proc. Combust. Inst.* **2015**, *35*, 3739–3747. [[CrossRef](#)]
43. Goldenstein, C.S.; Schultz, I.A.; Spearrin, R.M.; Jeffries, J.B.; Hanson, R.K. Diode Laser Measurements of Temperature and H₂O for Monitoring Pulse Detonation Combustor Performance. In Proceedings of the ICDEERS Conference, Taipei, Taiwan, 28 July–2 August 2013.

44. Spearrin, R.M.; Goldenstein, C.S.; Jeffries, J.B.; Hanson, R.K. Fiber-coupled 2.7 μm laser absorption sensor for CO_2 in harsh combustion environments. *Meas. Sci. Technol.* **2013**, *24*, 055107. [[CrossRef](#)]
45. Spearrin, R.M.; Goldenstein, C.S.; Jeffries, J.B.; Hanson, R.K. Quantum cascade laser absorption sensor for carbon monoxide in high-pressure gases using wavelength modulation spectroscopy. *Appl. Opt.* **2014**, *53*, 1938–1946. [[CrossRef](#)]
46. Goldenstein, C.S.; Almodóvar, C.A.; Jeffries, J.B.; Hanson, R.K.; Brophy, C.M. High-bandwidth scanned-wavelength-modulation spectroscopy sensors for temperature and H_2O in a rotating detonation engine. *Meas. Sci. Technol.* **2014**, *25*, 105104. [[CrossRef](#)]
47. Gordon, I.E.; Rothman, L.S.; Hill, C.; Kochanov, R.V.; Tan, Y.; Bernath, P.F.; Birk, M.; Boudon, V.; Campargue, A.; Chance, K.V.; et al. The HITRAN2016 molecular spectroscopic database. *J. Quant. Spectrosc. Radiat. Transf.* **2017**, *203*, 3–69. [[CrossRef](#)]
48. Chao, X. *Development of Laser Absorption Sensors for Combustion Gases*; Stanford University: Stanford, CA, USA, 2012.
49. Sanders, S.T.; Wang, J.; Jeffries, J.B.; Hanson, R.K. Diode-laser absorption sensor for line-of-sight gas temperature distributions. *Appl. Opt.* **2001**, *40*, 4404–4415. [[CrossRef](#)] [[PubMed](#)]
50. Liu, X.; Jeffries, J.B.; Hanson R, K. Measurements of spectral parameters of water-vapour transitions near 1388 and 1345 nm for accurate simulation of high-pressure absorption spectra. *Meas. Sci. Technol.* **2007**, *18*, 1185. [[CrossRef](#)]
51. Li, H.; Farooq, A.; Jeffries, J.B.; Hanson, R.K. Diode laser measurements of temperature-dependent collisional-narrowing and broadening parameters of Ar-perturbed H_2O transitions at 1391.7 and 1397.8 nm. *J. Quant. Spectrosc. Radiat. Transf.* **2008**, *109*, 132–143. [[CrossRef](#)]
52. Skrotzki, J.; Habig, J.C.; Ebert, V. Integrative fitting of absorption line profiles with high accuracy, robustness, and speed. *Appl. Phys. B* **2014**, *116*, 393–406. [[CrossRef](#)]
53. Abrarov, S.M.; Quine, B.M.; Jagpal R, K. A simple interpolating algorithm for the rapid and accurate calculation of the Voigt function. *J. Quant. Spectrosc. Radiat. Transf.* **2009**, *110*, 376–383. [[CrossRef](#)]
54. Pagnini, G.; Mainardi, F. Evolution equations for the probabilistic generalization of the Voigt profile function. *J. Comput. Appl. Math.* **2010**, *233*, 1590–1595. [[CrossRef](#)]
55. Rieker, G.B.; Jeffries, J.B.; Hanson R, K. Calibration-free wavelength-modulation spectroscopy for measurements of gas temperature and concentration in harsh environments. *Appl. Opt.* **2009**, *48*, 5546–5560. [[CrossRef](#)]
56. Liu, J.T.C. *Near-Infrared Diode Laser Absorption Diagnostics for Temperature and Species in Engines*; Stanford University: Stanford, CA, USA, 2004.
57. Zhou, X. *Diode Laser Absorption Sensors for Combustion Control*; Stanford University: Stanford, CA, USA, 2005.
58. Sun, K.; Chao, X.; Sur, R.; Goldenstein, C.S.; Jeffries, J.B.; Hanson, R.K. Analysis of calibration-free wavelength-scanned wavelength modulation spectroscopy for practical gas sensing using tunable diode lasers. *Meas. Sci. Technol.* **2013**, *24*, 125203. [[CrossRef](#)]
59. Goldenstein, C.S.; Strand, C.L.; Schultz, I.A.; Sun, K.; Jeffries, J.B.; Hanson, R.K. Fitting of calibration-free scanned-wavelength-modulation spectroscopy spectra for determination of gas properties and absorption lineshapes. *Appl. Opt.* **2014**, *53*, 356–367. [[CrossRef](#)]
60. Stewart, G.; Johnstone, W.; Bain, J.R.P.; Ruxton, K.; Duffin, K. Recovery of absolute gas absorption line shapes using tunable diode laser spectroscopy with wavelength modulation—Part I: Theoretical analysis. *J. Lightwave Technol.* **2011**, *29*, 811–821.
61. Bain, J.R.P.; Johnstone, W.; Ruxton, K.; Stewart, G.; Lengden, M.; Duffin, K. Recovery of absolute gas absorption line shapes using tunable diode laser spectroscopy with wavelength modulation—Part 2: Experimental investigation. *J. Lightwave Technol.* **2011**, *29*, 987–996. [[CrossRef](#)]
62. Peng, Z.; Ding, Y.; Che, L.; Yang, Q. Odd harmonics with wavelength modulation spectroscopy for recovering gas absorbance shape. *Opt. Express* **2012**, *20*, 11976–11985.
63. Klein, A.; Witzel, O.; Ebert, V. Rapid, time-division multiplexed, direct absorption-and wavelength modulation-spectroscopy. *Sensors* **2014**, *14*, 21497–21513. [[CrossRef](#)] [[PubMed](#)]
64. Liu, X.; Jeffries, J.B.; Hanson R, K. Measurement of non-uniform temperature distributions using line-of-sight absorption spectroscopy. *AIAA J.* **2007**, *45*, 411–419. [[CrossRef](#)]
65. Cai, W.; Kaminski C, F. Tomographic absorption spectroscopy for the study of gas dynamics and reactive flows. *Prog. Energy Combust. Sci.* **2017**, *59*, 1–31. [[CrossRef](#)]

66. Rieker, G.B.; Giorgetta, F.R.; Swann, W.C.; Kofler, J.; Zolot, A.M.; Sinclair, L.C.; Baumann, E.; Cromer, C.; Petron, G.; Tans, P.P.; et al. Frequency-comb-based remote sensing of greenhouse gases over kilometer air paths. *Optica* **2014**, *1*, 290–298. [CrossRef]
67. Malarich, N.A.; Rieker, G., B. Resolving gas temperature distributions with single-beam dual-comb absorption spectroscopy. In Proceedings of the Conference on Lasers and Electro-Optics (CLEO), San Jose, CA, USA, 14–19 May 2017.
68. Ma, L.; Cai, W.; Caswell, A.W.; Kraetschmer, T.; Sanders, S.T.; Roy, S.; Gord, J.R. Tomographic imaging of temperature and chemical species based on hyperspectral absorption spectroscopy. *Opt. Express* **2009**, *17*, 8602–8613. [CrossRef] [PubMed]
69. Ma, L.; Li, X.; Sanders, S.T.; Caswell, A.W.; Roy, S.; Plemmons, D.H.; Gord, J.R. 50-kHz-rate 2D imaging of temperature and H₂O concentration at the exhaust plane of a J85 engine using hyperspectral tomography. *Opt. Express* **2013**, *21*, 1152–1162. [CrossRef] [PubMed]
70. Mohammad, I.L.; Anderson, G.T.; Chen, Y. Noise estimation technique to reduce the effects of 1/f noise in Open Path Tunable Diode Laser Absorption Spectrometry (OP-TDLAS). In Proceedings of the Sensors for Extreme Harsh Environments. International Society for Optics and Photonics, Baltimore, MD, USA, 5–9 May 2014.
71. Werle, P.W.; Mazzinghi, P.; D'Amato, F.; De Rosa, M.; Maurer, K.; Slemr, F. Signal processing and calibration procedures for in situ diode-laser absorption spectroscopy. *Spectrochim. Acta Part A Mol. Biomol. Spectrosc.* **2004**, *60*, 1685–1705. [CrossRef]
72. Lins, B.; Zinn, P.; Engelbrecht, R.; Schmauss, B. Simulation-based comparison of noise effects in wavelength modulation spectroscopy and direct absorption TDLAS. *Appl. Phys. B* **2010**, *100*, 367–376. [CrossRef]
73. Zhu, J.; Cowie, A.; Kosterev, A.; Wyatt, D. Advantages of Using Direct Absorption Method for TDLAS Measurement. Available online: <https://zh.scribd.com/document/234114018/Paper-Advantages-of-Using-Direct-Absorption-Method-for-TDLAS-Measurement-r1> (accessed on 3 July 2019).
74. Hodgkinson, J.; Tatam, R.P. Optical gas sensing: A review. *Meas. Sci. Technol.* **2012**, *24*, 012004. [CrossRef]
75. Hodgkinson, J.; Masiyano, D.; Tatam, R.P. Gas cells for tunable diode laser absorption spectroscopy employing optical diffusers. Part 1: Single and dual pass cells. *Appl. Phys. B* **2010**, *100*, 291–302. [CrossRef]
76. Ehlers, P.; Johansson, A.C.; Silander, I.; Foltynowicz, A.; Axner, O. Use of etalon-immune distances to reduce the influence of background signals in frequency-modulation spectroscopy and noise-immune cavity-enhanced optical heterodyne molecular spectroscopy. *JOSA B* **2014**, *31*, 2938–2945. [CrossRef]
77. Bomse, D.S.; Stanton, A.C.; Silver, J.A. Frequency modulation and wavelength modulation spectroscopies: Comparison of experimental methods using a lead-salt diode laser. *Appl. Opt.* **1992**, *31*, 718–731. [CrossRef] [PubMed]
78. Chou, S.I.; Baer, D.S.; Hanson, R.K. Diode laser absorption measurements of CH₃Cl and CH₄ near 1.65 μm. *Appl. Opt.* **1997**, *36*, 3288–3293. [CrossRef] [PubMed]
79. Webster, C.R. Brewster-plate spoiler: A novel method for reducing the amplitude of interference fringes that limit tunable-laser absorption sensitivities. *JOSA B* **1985**, *2*, 1464–1470. [CrossRef]
80. Masiyano, D.; Hodgkinson, J.; Schilt, S.; Tatam, R.P. Self-mixing interference effects in tunable diode laser absorption spectroscopy. *Appl. Phys. B* **2009**, *96*, 863–874. [CrossRef]
81. Persson, L.; Andersson, F.; Andersson, M.; Svanberg, S. Approach to optical interference fringes reduction in diode laser absorption spectroscopy. *Appl. Phys. B* **2007**, *87*, 523–530. [CrossRef]
82. Kluczynski, P.; Lindberg, Å.M.; Axner, O. Characterization of background signals in wavelength-modulation spectrometry in terms of a Fourier based theoretical formalism. *Appl. Opt.* **2001**, *40*, 770–782. [CrossRef]
83. Xiong, B.; Du, Z.; Li, J. Modulation index optimization for optical fringe suppression in wavelength modulation spectroscopy. *Rev. Sci. Instrum.* **2015**, *86*, 113104. [CrossRef] [PubMed]
84. Sun, K.; Chao, X.; Sur, R.; Jeffries, J.B.; Hanson, R.K. Wavelength modulation diode laser absorption spectroscopy for high-pressure gas sensing. *Appl. Phys. B* **2013**, *110*, 497–508. [CrossRef]
85. Xia, H.; Dong, F.; Zhang, Z.; Tu, G.; Pang, T.; Wu, B.; Wang, Y. Signal analytical processing based on wavelet transform for tunable diode laser absorption spectroscopy. In Proceedings of the Advanced Sensor Systems and Applications IV. International Society for Optics and Photonics, Beijing, China, 2 November 2010.
86. Li, C.; Guo, X.; Ji, W.; Wei, J.; Qiu, X.; Ma, W. on fringe removal of tunable diode laser multi-pass spectroscopy by wavelet transforms. *Opt. Quant. Electron.* **2018**, *50*, 275. [CrossRef]

87. Niu, M.; Han, P.; Song, L.; Hao, D.; Zhang, J.; Ma, L. Comparison and application of wavelet transform and Kalman filtering for denoising in $\delta^{13}\text{CO}_2$ measurement by tunable diode laser absorption spectroscopy at 2.008 μm . *Opt. Express* **2017**, *25*, A896–A905. [CrossRef] [PubMed]
88. Tian, G.; Li, J. Tunable diode laser spectrometry signal de-noising using discrete wavelet transform for molecular spectroscopy study. *Opt. Appl.* **2013**, *43*. [CrossRef]
89. Yang, R.; Bi, Y.; Zhou, Q.; Dong, X.; Lv, T. A background reduction method based on empirical mode decomposition for tunable diode laser absorption spectroscopy system. *Optik* **2018**, *158*, 416–423. [CrossRef]
90. Uehara, K. Dependence of harmonic signals on sample-gas parameters in wavelength-modulation spectroscopy for precise absorption measurements. *Appl. Phys. B Lasers Opt.* **1998**, *67*, 517–523. [CrossRef]
91. Kluczynski, P.; Axner, O. Theoretical description based on Fourier analysis of wavelength-modulation spectrometry in terms of analytical and background signals. *Appl. Opt.* **1999**, *38*, 5803–5815. [CrossRef]
92. Neethu, S.; Verma, R.; Kamble, S.S.; Radhakrishnan, J.K.; Krishnapur, P.P.; Padaki, V.C. Validation of wavelength modulation spectroscopy techniques for oxygen concentration measurement. *Sens. Actuators B Chem.* **2014**, *192*, 70–76. [CrossRef]
93. Fried, A.; Henry, B.; Drummond, J.R. Tunable diode laser ratio measurements of atmospheric constituents by employing dual fitting analysis and jump scanning. *Appl. Opt.* **1993**, *32*, 821–827. [CrossRef]
94. Chen, J.; Hangauer, A.; Strzoda, R.; Amann, M.C. Tunable diode laser spectroscopy with optimum wavelength scanning. *Appl. Phys. B* **2010**, *100*, 331–339. [CrossRef]
95. Du, Z.; Yan, Y.; Li, J.; Zhang, S.; Yang, X.; Xiao, Y. In situ, multiparameter optical sensor for monitoring the selective catalytic reduction process of diesel engines. *Sens. Actuators B Chem.* **2018**, *267*, 255–264. [CrossRef]
96. Peng, W.Y.; Sur, R.; Strand, C.L.; Spearrin, R.M.; Jeffries, J.B.; Hanson, R.K. High-sensitivity in situ QCLAS-based ammonia concentration sensor for high-temperature applications. *Appl. Phys. B* **2016**, *122*, 188. [CrossRef]
97. Sur, R.; Peng, W.Y.; Strand, C.; Spearrin, R.M.; Jeffries, J.B.; Hanson, R.K.; Bekal, A.; Halder, P.; Poonacha, S.P.; Vartak, S.; et al. Mid-infrared laser absorption spectroscopy of NO₂ at elevated temperatures. *J. Quant. Spectrosc. Radiat. Transf.* **2017**, *187*, 364–374. [CrossRef]
98. Li, J.; Yu, B.; Fischer, H. Wavelet transform based on the optimal wavelet pairs for tunable diode laser absorption spectroscopy signal processing. *Appl. Spectrosc.* **2015**, *69*, 496–506. [CrossRef] [PubMed]
99. Weisberger, J.M.; Richter, J.P.; Parker, R.A.; DesJardin, P.E. Direct absorption spectroscopy baseline fitting for blended absorption features. *Appl. Opt.* **2018**, *57*, 9086–9095. [CrossRef]
100. Chen, J.; Hangauer, A.; Strzoda, R.; Amann, M.C. VCSEL-based calibration-free carbon monoxide sensor at 2.3 μm with in-line reference cell. *Appl. Phys. B* **2011**, *102*, 381–389. [CrossRef]
101. Qu, Z.; Ghorbani, R.; Valiev, D.; Schmidt, F.M. Calibration-free scanned wavelength modulation spectroscopy—application to H₂O and temperature sensing in flames. *Opt. Express* **2015**, *23*, 16492–16499. [CrossRef]
102. Zhao, G.; Tan, W.; Hou, J.; Qiu, X.; Ma, W.; Li, Z.; Axner, O. Calibration-free wavelength-modulation spectroscopy based on a swiftly determined wavelength-modulation frequency response function of a DFB laser. *Opt. Express* **2016**, *24*, 1723–1733. [CrossRef]
103. Upadhyay, A.; Lengden, M.; Wilson, D.; Humphries, G.S.; Crayford, A.P.; Pugh, D.G.; Johnstone, W. A new RAM normalized 1f-WMS technique for the measurement of gas parameters in harsh environments and a comparison with 2f/1f. *IEEE Photonics J.* **2018**, *10*, 1–11. [CrossRef]
104. Upadhyay, A.; Wilson, D.; Lengden, M.; Chakraborty, A.L.; Stewart, G.; Johnstone, W. Demonstration of Calibration-Free WMS Measurement of Gas Parameters with in-Situ Real-Time Characterization of Laser Parameters Using CW-DFB-QCL, VCSEL and DFB Lasers. 2016. Available online: <https://core.ac.uk/download/pdf/77036446.pdf> (accessed on 3 July 2019).
105. Upadhyay, A.; Wilson, D.; Lengden, M.; Chakraborty, A.L.; Stewart, G.; Johnstone, W. Calibration-free WMS using a cw-DFB-QCL, a VCSEL, and an edge-emitting DFB laser with in-situ real-time laser parameter characterization. *IEEE Photonics J.* **2017**, *9*, 1–17. [CrossRef]
106. Upadhyay, A.; Chakraborty, A.L. Calibration-free 2f WMS with in situ real-time laser characterization and 2f RAM nulling. *Opt. Lett.* **2015**, *40*, 4086–4089. [CrossRef] [PubMed]
107. Zhai, B.; He, Q.; Huang, J.; Zheng, C.; Wang, Y. Design and realization of harmonic signal orthogonal lock-in amplifier used in infrared gas detection. *Acta Photonica Sin.* **2014**, *43*, 1125001. [CrossRef]

108. Jiang, C.; Liu, Y.; Yu, B.; Yin, S.; Chen, P. TDLAS-WMS second harmonic detection based on spectral analysis. *Rev. Sci. Instrum.* **2018**, *89*, 083106. [[CrossRef](#)] [[PubMed](#)]
109. Du, Y.; Peng, Z.; Ding, Y. Wavelength modulation spectroscopy for recovering absolute absorbance. *Opt. Express* **2018**, *26*, 9263–9272. [[CrossRef](#)] [[PubMed](#)]
110. Duan, H.; Gautam, A.; Shaw, B.D.; Cheng, H. Harmonic wavelet analysis of modulated tunable diode laser absorption spectroscopy signals. *Appl. Opt.* **2009**, *48*, 401–407. [[CrossRef](#)] [[PubMed](#)]



© 2019 by the authors. Licensee MDPI, Basel, Switzerland. This article is an open access article distributed under the terms and conditions of the Creative Commons Attribution (CC BY) license (<http://creativecommons.org/licenses/by/4.0/>).